Inorganic Chemistry
Article

Inorg. Chem. **2010**, *49*, 745–751 **745**
DOI: 10.1021/ic902161v

Pressure Effects on a Spin-Crossover Monomeric Compound [Fe(pmea)(SCN)$_2$] (pmea = bis[(2-pyridyl)methyl]-2-(2-pyridyl)ethylamine)

Bao Li, Rong-Jia Wei, Jun Tao,* Rong-Bin Huang, and Lan-Sun Zheng

State Key Laboratory of Physical Chemistry of Solid Surfaces and Department of Chemistry, College of Chemistry and Chemical Engineering, Xiamen University, Xiamen 361005, People's Republic of China

Received November 2, 2009

Spin-crossover (SCO) compounds are a sort of bistable material whose electronic and magnetic properties can be tuned by external physical stimuli, such as heat, light, and pressure. The title SCO compound [Fe(pmea)(NCS)$_2$] (**1**; pmea = bis[(2-pyridyl)methyl]-2-(2-pyridyl)ethylamine) undergoes spin transition in such a way that it is an ideal candidate to investigate pressure effects on the SCO behavior. First, the spin transition is complete and abrupt so that the pressure-dependent spin transition should be remarkable. Second, the $T_{1/2}$ value under ambient pressure is 184 K, which guarantees that the SCO temperature under various pressures does not exceed that restrained by high-pressure devices. The magnetic data of compound **1** under different external pressures were analyzed through a known method, as reported by Gütlich, which gave an interaction parameter Γ of 264(5) cm^{-1} and a volume change $\Delta V°_{HL}$ of 32(3) Å^3 molecule^{-1} [HL represents a high-spin (HS) ↔ low-spin (LS) transition], respectively. Meanwhile, the calculated entropy change $\Delta S°_{HL}(T)$ at 1 bar is 59.79 J mol^{-1} K^{-1}, which is a typical value that drives the spin transition from a LS to HS state. The pressure effects on the SCO behavior of compound **1** reported here may provide information for a deep understanding of the correlation between pressure and spin transition.

Introduction

Bistable molecule-based materials whose electronic and magnetic properties can often be affected by external physical stimuli have been attracting great attention because of their potential applications,[1] which mainly includes the extensively studied spin-crossover (SCO)[2] and valence tautomeric[3] compounds. Because of the clear change of properties, especially the color and magnetism change, along with the conversion between two different electronic spin states, those materials are suggested to be useful in applications as molecular switches and sensors, for information storage, and in display technologies.[4]

Up to now, numerous SCO compounds, mostly incorporating compounds of Fe^{II}, Fe^{III}, and Co^{II}, have been synthesized and carefully characterized.[5] Over these extensive studies, it has become clear that SCO behaviors are fundamentally associated with intermolecular interactions as well as the ligand-field strength found in the solid state, which contributes to the cooperativity between the SCO units that influences the spin transition.[6] In Fe^{II} SCO compounds, the reversible spin transition ascribes to a transformation between high-spin (HS) and low-spin (LS) states, $(t_{2g})^4(e_g)^2 \leftrightarrow (t_{2g})^6(e_g)^0$, accompanied by a change of the metal−ligand bond length of about 0.2 Å, which causes the molecular size in the HS state to be larger than that in the LS state by 3−5%.[7] Because of the volume change between LS and HS

*To whom correspondence should be addressed. E-mail: taojun@xmu.edu.cn.

(1) (a) Kahn, O.; Launay, J. P. *Chemtronics* **1988**, *3*, 140–151. (b) Kahn, O.; Kröber, J.; Jay, C. *Adv. Mater.* **1992**, *4*, 718–728. (c) Sato, O.; Iyoda, T.; Fujishima, A.; Hashimoto, K. *Science* **1996**, *272*, 704–745.

(2) (a) Gütlich, P., Goodwin, H. A., Eds. Spin Crossover in Transition Metal Compounds I. *Topics in Current Chemistry*; Springer: New York, 2004; Vol. *233*. (b) Gütlich, P.; Dei, A. *Angew. Chem., Int. Ed.* **1997**, *36*, 2734–2737.

(3) (a) Miller, J. S., Drillon, M., Eds. *Magnestism: Molecules to Materials IV*; Wiley-VCH: Weinheim, Germany, 2002. (b) Real, J. A.; Gaspar, A. B.; Niel, V.; Muñoz, M. C. *Coord. Chem. Rev.* **2003**, *236*, 121–141. (c) Sato, O.; Tao, J.; Zhang, Y. Z. *Angew. Chem., Int. Ed.* **2007**, *46*, 2152–2187.

(4) (a) Gütlich, P.; Garcia, Y.; Woike, T. *Coord. Chem. Rev.* **2001**, *219*−*221*, 839–879. (b) Gaspar, A. B.; Ksenofontov, V.; Seredyuk, M.; Gütlich, P. *Coord. Chem. Rev.* **2005**, *249*, 2661–2676.

(5) (a) Gütlich, P.; Garcia, Y.; Goodwin, H. A. *Chem. Soc. Rev.* **2000**, *29*, 419–427. (b) Bai, Y. L.; Tao, J.; Huang, R. B.; Zheng, L. S.; Zheng, S. L.; Oshida, K.; Einaga, Y. *Chem. Commun.* **2008**, 1753–1755. (c) Tao, J.; Maruyama, H.; Sato, O. *J. Am. Chem. Soc.* **2006**, *128*, 1790–1791. (d) Li, B.; Tao, J.; Sun, H. L.; Sato, O.; Huang, R. B.; Zheng, L. S. *Chem. Commun.* **2008**, 2269–2271. (e) Li, B.; Yang, F. L.; Tao, J.; Sato, O.; Huang, R. B.; Zheng, L. S. *Chem. Commun.* **2008**, 6019–6021. (f) Bonnet, S.; Molnár, G.; Costa, J. S.; Siegler, M. A.; Spek, A. L.; Bousseksou, A.; Fu, W. T.; Gamez, P.; Reedijk, J. *Chem. Mater.* **2009**, *21*, 1123–1136.

(6) (a) Halder, G. J.; Kepert, C. J.; Moubaraki, B.; Murray, K. S.; Cashion, J. D. *Science* **2002**, *298*, 1762–1765. (b) Kepenekian, M.; Guennic, B. L.; Robert, V. *J. Am. Chem. Soc.* **2009**, *131*, 11498–11502. (c) Ksenofontov, V.; Gaspar, A. B.; Niel, V.; Reiman, S.; Real, J. A.; Gütlich, P. *Chem.—Eur. J.* **2004**, *10*, 1291–1298.

(7) (a) Shultz, D. A. In *Magnetism: Molecules to Materials II*; Miller, J. S., Drillon, M., Eds.; Wiley-VCH: Weinheim, Germany, 2001; pp 281−306. (b) Gütlich, P.; Goodwin, H. A. *Top. Curr. Chem.* **2004**, *234*, 1–276. (c) Murray, K. S.; Kepert, C. J. *Top. Curr. Chem.* **2004**, *233*, 195–228. (d) Létard, J. F.; Guionneau, P.; Goux-Capes, L. *Top. Curr. Chem.* **2004**, *235*, 221–249.

© 2009 American Chemical Society
Published on Web 12/21/2009

states, the hydrostatic pressure could be one approach that effectively modifies the behavior of the SCO compounds. It is now well-known that most SCO compounds are pressure-sensitive; plenty of experiments have revealed that an increase of the external pressure would favor the LS state and, as a consequence, the transition temperature increases. The reason is mostly that the application of external pressure increases the zero-point energy difference $\Delta E°$ and decreases the activation energy $\Delta W°$, thus favoring the LS state.[8]

Recently, theoretical studies also indicate that the thermodynamic properties and microscopic mechanism of spin transition in the solid state could be investigated by the application of pressure along with the development of hydrostatic pressure cells in connection with magnetic susceptibility. Following theoretical approaches, systematic investigations on **1** under different external pressure were performed, and a suitable actual model for investigating pressure effects on the SCO compound is established, which would provide abundant and authentic information for an understanding of the correlation between the pressure and spin transition.

The title compound [Fe(pmea)(NCS)$_2$] (**1**; pmea = bis[(2-pyridyl)methyl]-2-(2-pyridyl)ethylamine) has been studied by IR and Raman spectroscopy and density functional theory calculations, which confirmed its SCO property;[9] however, unfortunately the crystal structure and detailed magnetic properties (SCO) were unknown. As our successive studies of pressure effects on the SCO behavior, we try to obtain single crystals of the title compounds and investigate its pressure-dependent magnetic properties. Here, we report the synthesis and variable-temperature crystal structures of compound **1** and especially its SCO behavior under variable pressures. It has been found that compound **1** undergoes a steep and complete spin transition with a $T_{1/2}$ value of 184 K under atmospheric pressure. More important is that, because of the complete and abrupt spin transition, compound **1** is an ideal candidate to study pressure effects on the SCO behavior.

Results and Discussion

Crystal Structures. Structural analyses of **1** were carried out under different temperatures in order to correlate, at the corresponding temperatures (at 120 and 260 K, respectively), the spin states of the Fe^{II} centers of the respective compounds with their structural parameters. Crystal data of **1** at different temperatures are gathered in Table 1, and selected bond lengths, angles, and structural parameters are summarized in Table 2.

Compound **1** crystallizes in the orthorhombic space group $Pc2_1n$, and the asymmetric unit contains one complete C_1-symmetric molecule **1**, as shown in Figure 1a. The neutral unit contains a tetradentate tripodal ligand pmea, one Fe^{II} ion, and two NCS^- groups, where only the cis configuration of NCS^- groups were observed because of the strain effect caused by the pmea ligand.[10] The Fe^{II} center is coordinated by six N atoms, four from the pmea ligand and two from the NCS^- groups. The axial positions of the coordination octahedron of the Fe^{II} atom are occupied by one of the NCS^- groups associated with the N5 atom and the aliphatic nitrogen, N4, while the equatorial plane is formed by one NCS^- group (N6), two pyridinato N atoms (N1 and N2) connected to N4 by the $-CH_2-$ group, and one pyridinato N atom (N3) connected to N4 by the $-CH_2CH_2-$ group. In the crystal structure, if the S1···Fe···S2 plane and S2···Fe···N2(pyridine) entity were viewed as symmetric mirror and rotation axes, respectively, the Fe(pmea)(NCS)$_2$ molecules then arranged in such a way that each molecule could be obtained from its adjacent one by mirror-symmetric operation and then rotation by 90°, as shown in Figure 1b. At 120 K, the average Fe−N bond length is 1.986(3) Å within a 1.938(2)−2.042(2) Å range, in accordance with the typical LS

Table 1. Crystallographic Data for **1**

	T/K	
	120	260
formula	$C_{21}H_{20}N_6S_2Fe_1$	
M_r/g mol^{-1}	476.40	
cryst syst	orthorhombic	
space group	$Pc2_1n$	
a/Å	10.451(1)	10.828(2)
b/Å	13.313(1)	13.653(2)
c/Å	14.991(1)	15.313(3)
V/Å^3	2085.7(1)	2263.8(6)
Z	4	4
D_c/g cm^{-3}	1.517	1.398
μ(Mo Kα)/mm^{-1}	0.945	0.870
F(000)	984	984
indep reflns	2950	3052
R1 [$F^2 > 2\sigma(F)^2$]	0.0234	0.0344
wR2 (F^2)	0.0575	0.0739

Table 2. Selected Bond Lengths [Å] and Angles [deg] for **1**[a]

	120 K	260 K
Fe1−N1	1.985(2)	2.192(3)
Fe1−N2	1.973(3)	2.212(2)
Fe1−N3	2.006(2)	2.189(3)
Fe1−N4	2.042(2)	2.266(3)
Fe1−N5	1.938(2)	2.060(3)
Fe1−N6	1.971(2)	2.125(3)
N1−Fe1−N2	92.5(1)	92.0(1)
N2−Fe1−N3	90.3(1)	86.7(1)
N1−Fe1−N5	92.7(1)	96.3(1)
N3−Fe1−N6	89.3(1)	90.2(1)
N5−Fe1−N6	87.9(1)	94.3(1)
N1−Fe1−N4	80.3(1)	74.5(1)
N2−Fe1−N4	83.4(1)	75.8(1)
N3−Fe1−N4	94.1(1)	89.3(1)
$\langle d_{Fe-N}\rangle$ [Å]	1.986(2)	2.174(3)
$\sum_{Fe}$ [deg]	43.0	61.6
S1···H−C in the *ac* plane [Å]	3.019(1)	3.165(2)
S2···H−C in the *ac* plane [Å]	2.902(1)	3.010(2)
S1···H−C in the *bc* plane [Å]	2.779(2)	3.016(2)
	2.872(2)	2.837(2)
$\pi-\pi$ in the *bc* plane [Å]	4.128(2)	4.089(2)
Fe···Fe distance in the *ac* plane [Å]	8.797(1)	8.930(2)
Fe···Fe distance in the *bc* plane [Å]	7.704(2)	7.760(2)

[a] $\langle d_{Fe-N}\rangle$ is the average Fe−N distance. $\sum_{Fe}$ is the sum of the deviations of cis N−Fe−N angles from 90°.

(8) Gütlich, P.; Gaspar, A. B.; Garcia, Y.; Ksenofontov, V. *C. R. Chim.* **2007**, *10*, 21–36.
(9) Brehm, G.; Reiher, M.; Guennic, B. L.; Leibold, M.; Schindler, S.; Heinemann, F. W.; Schneider, S. *J. Raman Spectrosc.* **2006**, *37*, 108–122.
(10) Matouzenko, G. S.; Bousseksou, A.; Lecocq, S.; Van Koningsbruggen, P. J.; Perrin, M.; Kahn, O.; Collet, A. *Inorg. Chem.* **1997**, *36*, 2975–2981.

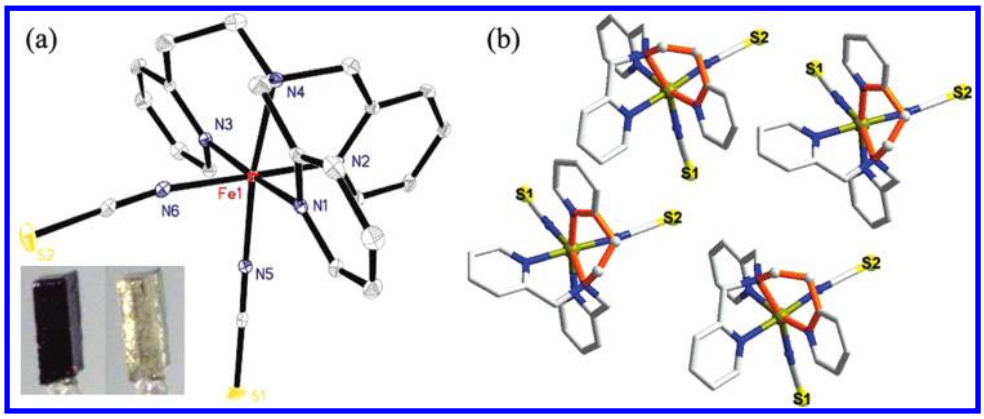

Figure 1. (a) Molecular structure of **1** at 120 K. Thermal ellipsoids are drawn at the 30% probability level. H atoms are omitted for clarity. (b) Representation of the adjacent units in one crystal showing different orientations with regard to the six-membered chelate rings associated with Fe1, N3, and N4.

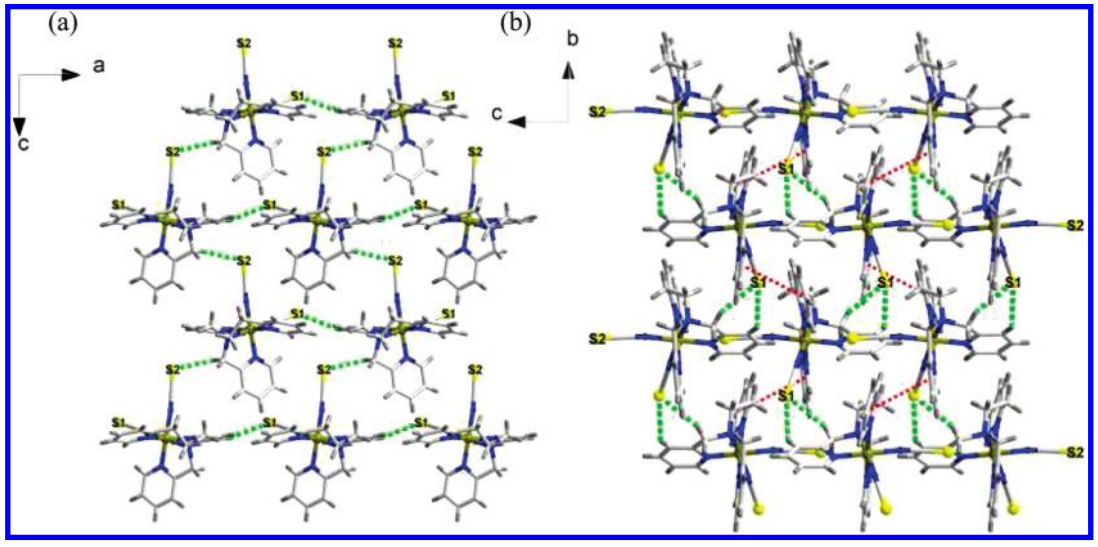

Figure 2. (a) Perspective view of the S···H−C interactions in the *ac* plane. (b) Perspective view of the S···H−C and $\pi-\pi$ interactions (red dotted lines) in the *bc* plane.

Fe^{II}−N bond lengths.[11] The slightly longer Fe−N bond lengths of Fe−N3 2.006(2) Å and Fe−N4 2.042(2) Å in the LS Fe^{II} state are mostly caused by the steric strains originating from substitution of the five-membered chelate ring by a six-membered one,[12] while at 260 K, where magnetic susceptibility shows that compound **1** has been in the HS state (see below), the average Fe−N bond length of 2.174(3) Å falls in the range of a value typical of HS Fe^{II}−N bonds.[11] Generally, the typical average variation of the Fe−N bond lengths is about 0.20 Å along with conversion between HS and LS states in SCO compounds. Here, the change values of four $Fe-N_{pmea}$ bonds are in the range of 0.20−0.24 Å (average 0.22 Å, Table 2); however, the average variation value of the $Fe-N_{NCS}$ bonds is only 0.14 Å, which is much smaller than that of the $Fe-N_{pmea}$ bonds. This difference is also observed in other SCO compounds containing $Fe-N_{NCS}$ bonds, whose variation is even about 0.1 Å.[13]

In the structure of molecule **1**, the FeN_6 coordination octahedron is highly distorted, whose angular deviation from an ideal octahedron can be commonly quantified by an octahedral distortion parameter, $\sum$ (sum of the deviations of cis N−Fe−N angles from 90°);[14] a smaller value is generally associated with a stronger ligand field and, consequently, a LS state, while the opposite holds true for a HS state.[11,14] In the present case, the values of 43.0° and 61.6° at 120 and 260 K, respectively, indicate that the ligand field at low temperature is much stronger than that at high temperature, implying LS and HS states, respectively, as confirmed by magnetic characterization.

The two-dimensional (2D) stacking structures showing S1···H−C and S2···H−C interactions in the *ac* plane and S1···H−C interactions in the *bc* plane, respectively, are shown in Figure 2. The 2D layer viewed along the *ac* plane (Figure 2a) displays strong S···H−C hydrogen bonds[15] with distances of 2.902(1) and 3.019(2) Å at 120 K and of 3.010(2) and 3.165(2) Å at 260 K (Table 2),

(11) Guionneau, P.; Marchivie, M.; Bravic, G.; Létard, J. F.; Chasseau, D. *Top. Curr. Chem.* **2004**, *234*, 97–128.
(12) Matouzenko, G. S.; Bousseksou, A.; Lecocq, S.; Van Koningsbruggen, P. J.; Perrin, M.; Kahn, O.; Collet, A. *Inorg. Chem.* **1997**, *36*, 5869–5879.
(13) Gallois, B.; Real, J. A.; Hauw, C.; Zarembowitch, J. *Inorg. Chem.* **1990**, *29*, 1152–1158.
(14) Guionneau, P.; Marchivie, M.; Bravic, G.; Létard, J. F.; Chasseau, D. *J. Mater. Chem.* **2002**, *12*, 2546–2551.
(15) (a) Amoore, J. J. M.; Kepert, C. J.; Cashion, J. D.; Moubaraki, B.; Neville, S. M.; Murray, K. S. *Chem.—Eur. J.* **2006**, *12*, 8220–8227. (b) Neville, S. M.; Leita, B. A.; Halder, G. J.; Kepert, C. J.; Moubaraki, B.; Létard, J. F.; Murray, K. S. *Chem.—Eur. J.* **2008**, *14*, 10123–10133.

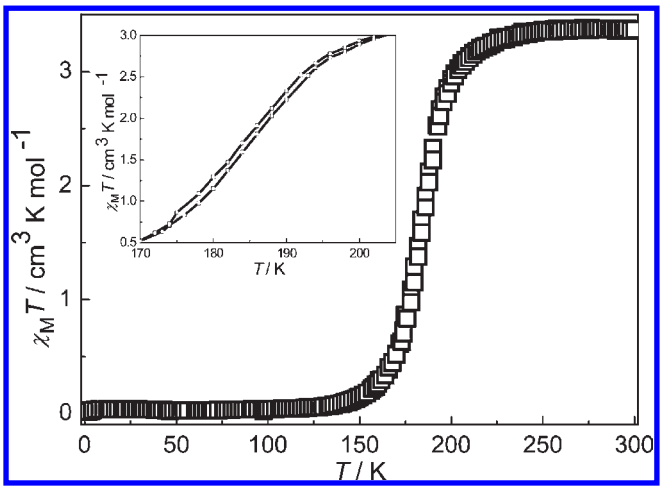

Figure 3. $\chi_M T$ versus T plots of **1** in the temperature range of 2−300 K. A small hysteresis with a width of 1 K is shown in the inset.

respectively, between adjacent molecules **1**, each one of which forms four hydrogen bonds by acting as two hydrogen-bond donors and two hydrogen-bond acceptors. Such 2D layers in the *ac* plane are connected along the [010] direction by two more S1···H−C interactions to form a compact 3D crystal structure. When viewed along the *bc* plane (Figure 2b), the distances of S1···H−C hydrogen bonds vary from 2.779(2) and 2.872(2) Å at 120 K to 3.016(2) and 2.837(2) Å at 260 K, respectively. In the *bc* plane, a moderate $\pi-\pi$ interaction with a centroid-to-centroid distance of 4.128(2) and 4.089(2) Å at 120 and 260 K (Table 2), respectively, is also found. However, no S···S interactions were observed. On the other hand, adjacent molecules **1** are stacked in the solid state by these relatively strong and complicated intermolecular interactions that give shortest Fe···Fe distances from 7.704(2) Å at 120 K to 7.760(2) Å at 260 K in the *bc* plane and from 8.797(1) to 8.930(2) Å in the *ac* plane, respectively. The ordered $\pi-\pi$ and S···H−C interactions in **1** are expected to drive the crystal packing that influences the SCO behavior through intermolecular "chemical pressure",[16] which is often affected by the external pressure.

Magnetic Properties under Pressure. The $\chi_M T$ versus T plots of compound **1** under ambient air pressure are shown in Figure 3. The $\chi_M T$ value of 3.37 cm^3 K mol^{-1} at room temperature corresponds to a HS Fe^{II} ion, which is slightly higher than the one expected for a spin-only HS Fe^{II} ion with $g = 2.0$, which is probably due to the results of an orbital contribution to the paramagnetic susceptibility. Upon cooling, the $\chi_M T$ value slowly decreases from 240 to 210 K and then goes abruptly to 150 K. Between this point and 2 K, the $\chi_M T$ values remain almost constant, with a remnant of 0.01 cm^3 K mol^{-1} that is ascribed to the contribution from the temperature-independent paramagnetism of the LS Fe^{II} molecule. The $\chi_M T$ values in the whole temperature range indicate that the spin transition is practically complete and centered at 184 K ($T_{1/2}\downarrow$) and 185 K ($T_{1/2}\uparrow$) in the cooling and warming modes, respectively, to give a small thermal hysteresis loop with a width of 1 K (Figure 3, inset). Because of the

(16) (a) Hauser, A. *Top. Curr. Chem.* **2004**, *234*, 155–198. (b) Spiering, H. *Top. Curr. Chem.* **2004**, *235*, 171–195.

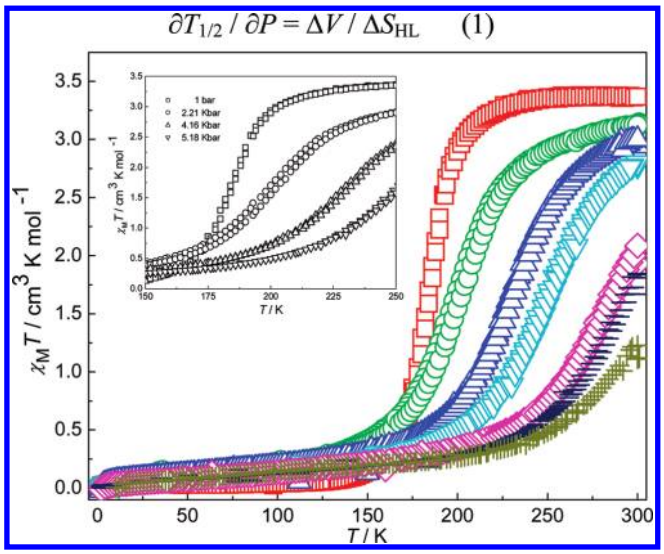

Figure 4. Pressure effects on the SCO behavior of **1** under 0.001 (□), 2.21 (○), 4.16 (△), 5.18 (▽), 7.27 (◇), 8.04 (—), and 9.17 (+) kbar, respectively. Inset: Slight increase of the hysteresis width under 2.21 and 4.16 kbar.

complete and abrupt SCO characteristics with a suitable transition temperature range, the mononuclear SCO compound **1** can be viewed as an ideal model to systematically and theoretically investigate the SCO behavior under external pressures.

In order to observe the pressure effects on the spin transition of compound **1**, the variable-temperature magnetic susceptibilities were measured under hydrostatic pressures between 1.0 and 10 kbar, and the $\chi_M T$ versus T plots of **1** under different external pressures are shown in Figure 4.

The spin transition under pressure undergoes two main changes. First, the spin transition moves progressively to a higher temperature range and the transition becomes more and more gradual as the external pressure increases; as a consequence, the HS population at room temperature decreases. Second, the hysteresis width slightly increases to about 4 K under 2.21 kbar ($T_{1/2}\downarrow$ = 199 K and $T_{1/2}\uparrow$ = 203 K) and 2 K under 4.16 kbar ($T_{1/2}\downarrow$ = 230 K and $T_{1/2}\uparrow$ = 232 K) but recovers to 1 K under 5.18 kbar (Figure 4, inset). When the pressure rises to 9.17 kbar, the compound is almost in the LS state at room temperature. In order to qualitatively interpret the effect of the external pressure on the SCO behavior, the mean-field theory was used.[17] The relationship between the external pressure and the transition temperature under mean-field approximation obeys the Clausius−Clapeyron equation (eq 1), which reflects the scaling of the transition temperature $T_{1/2}$ and the volume change ΔV along with the change of the external pressure:

$$\partial T_{1/2}/\partial P = \Delta V/\Delta S_{HL} \quad (1)$$

For compound **1**, the transition temperatures $T_{1/2}$ under different external pressures in the cooling mode

(17) (a) Meissner, E.; Köppen, H.; Spiering, H.; Gütlich, P. *Chem. Phys. Lett.* **1983**, *95*, 163–166. (b) Spiering, H.; Meissner, E.; Köppen, H.; Müller, E. W.; Gütlich, P. *Chem. Phys.* **1982**, *68*, 65–71. (c) Adler, P.; Wiehl, L.; Meissner, E.; Köppen, C. P.; Spiering, H.; Gütlich, P. *J. Phys. Chem. Solids* **1987**, *48*, 517–525.

Table 3. $T_{1/2}$ at Different External Pressures

P (kbar)	$T_{1/2}$ (K)	P (kbar)	$T_{1/2}$ (K)
0.001	184	7.27	286
2.21	199	8.04	294
4.16	230	9.17	
5.18	251		

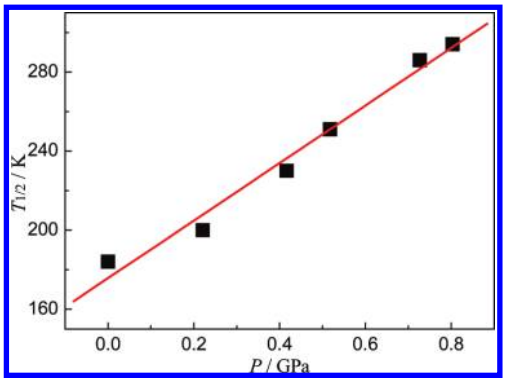

Figure 5. $T_{1/2}$ versus P plots for **1**. A linear fit to the data (—) gives a slope of 146 K GPa^{-1} (R^2 = 0.99).

are listed in Table 3, and plots of the transition temperature $T_{1/2}$ versus external pressure P are shown in Figure 5, which shows a good linear dependence. The first-order fitting gives a slope of 146 K GPa^{-1} with R^2 = 0.99, which is close to the values of 150, 160, and 176 K GPa^{-1} for mononuclear compounds $[Fe(2\text{-pic})_3]Cl_2 \cdot EtOH$ (2-pic = 2-picolylamine),[18] $[Fe(PM\text{-}aza)_2(NCS)_2]$ [PM-aza = *N*-(2′-pyridylmethylene)-4-azophenylaniline],[19] and $[Fe(abpt)_2(NCS)_2]$ [abpt = 4-amino-3,5- bis(pyridin-2-yl)-1,2,4-triazole],[20] respectively. Thus, the effect of the external pressure on the spin transition of compound **1** can be interpreted by the method based on the phenomenological theory of phase transitions in SCO systems.[21] However, some examples that exhibit nonlinear behavior of $T_{1/2}$ versus P have also been reported, which is mostly caused by different compressibilities of the large ions[21d] or the occurrence of a crystallographic phase transition[21e] under the application of external pressure. Here, compound **1**, because of the compact crystal packing and unchanged crystallographic phase between the LS and HS states, exhibits thus a linear dependence of $T_{1/2}$ versus P as general reports.[21] Whatever, if a more detailed crystallographic study of the SCO compound under variable external pressure and temperature were obtained, a quantitative interpretation of the influence of external pressure on the SCO transition would come true.

Thermodynamics. On the basis of the theory of thermodynamics, the Gibbs free energy of a thermally induced SCO system is in correlation with a random distribution of γ_{HS}, the magnitude of the volume change of the unit cell per SCO complex, $\Delta V^\circ_{HL} = V^\circ_{HS} - V^\circ_{LS}$, and all of the intermolecular interaction free energies between the spin-changing molecules, G_{int}, which could be written as eq 2:[17,21,22]

$$G(\gamma_{HS}, p, T) = \gamma_{HS}[\Delta F^\circ_{HL}(T) + p\Delta V^\circ_{HL}(T)] - TS_{mix}(\gamma_{HS}) + G_{int}(\gamma_{HS}) \quad (2)$$

in which all γ_{HS}-independent terms have been omitted and $\Delta F^\circ_{HL}(T)$ equals $F^\circ_{HS}(T) - F^\circ_{LS}(T)$ corresponding to the free energy difference between the HS and LS states during the spin transition at 1 bar, while $S_{mix} = -k_\beta[\gamma_{HS} \ln(\gamma_{HS}) + (1 - \gamma_{HS}) \ln(1 - \gamma_{HS})]$ is the mixing entropy (k_β, Boltzmann constant).

In the mean-field approximation, $G_{int}(\gamma_{HS})$ can be expanded in the following form:[17,21,22]

$$G_{int}(\gamma_{HS}) = \Delta_s\gamma_{HS} - \Gamma\gamma_{HS}^2 \quad (3)$$

The interaction parameter Γ describes the interaction between the HS and LS entities, and the lattice energy shift Δ_s depends on their interaction with the reference lattice under the condition that the lattice is in thermal equilibrium:

$$(\partial G/\partial\gamma_{HS})_{T,P} = 0 \quad (4)$$

Finally, the effect of external pressure on SCO can result in the implicit equation of state

$$\Delta F^\circ_{HL}(T) + p\Delta V^\circ_{HL} + \Delta_s - 2\Gamma\gamma_{HS} + k_\beta T \ln[\gamma_{HS}/(1 - \gamma_{HS})] = 0 \quad (5)$$

When calculated through use of the method introduced by Hauser et al.,[23] the values of ΔV°_{HL} and Γ can be determined using eq 5 and the γ_{HS} data can be obtained from measurements under different pressures without any prior knowledge of $\Delta F^\circ_{HL}(T)$ and Δ_s. In the following, the temperature dependence of Δ_s and Γ is assumed to be negligible.[17] At a given temperature and two different external pressures, eq 5 could be transformed into the following relationship:[24]

$$(p2 - p1)\Delta V^\circ_{HL} - 2\Gamma[\gamma_{HS}(p2, T) - \gamma_{HS}(p1, T)] = -k_\beta T \ln\{\gamma_{HS}(p2, T)\,[1 - \gamma_{HS}(p1, T)]/[1 - \gamma_{HS}(p2, T)]\gamma_{HS}(p1, T)\} \quad (6)$$

The right part of eq 6 and $\gamma_{HS}(p2,T) - \gamma_{HS}(p1,T)]$ are thought to be the two variables Y and X, respectively, and the plots of Y versus X obtained from the transition curves for $p2$ = 2210 bar and $p1$ = 1 bar and for $p2$ = 4160 bar and $p1$ = 1 bar, respectively, are shown in Figure 6. A well-linear fit to the experimental points gives mean

(18) Romstedt, H.; Hauser, A.; Spiering, H. *J. Phys. Chem. Solids* **1998**, *59*, 265–275.
(19) Ksenofontov, V.; Levchenko, G. G.; Spiering, H.; Gütlich, P.; Létard, J. F.; Bouhedja, Y.; Kahn, O. *Chem. Phys. Lett.* **1998**, *294*, 545–553.
(20) (a) Gaspar, A. B.; Muñoz, M. C.; Moliner, N.; Ksenofontov, V.; Levchenko, G. G.; Gütlich, P.; Real, J. A. *Monatsh. Chem.* **2003**, *134*, 285–294. (b) Gaspar, A. B.; Muñoz, M. C.; Moliner, N.; Ksenofontov, V.; Levchenko, G. G.; Gütlich, P.; Real, J. A. Molecular Magnets. In *Recent Highlights*; Linert, W., Verdaguer, M., Eds.; Springer-Verlag: New York, 2003; Vol. *169*, p 178.
(21) (a) Köhler, C. P.; Jakobi, R.; Meissner, E.; Wiehl, L.; Spiering, H.; Gütlich, P. *J. Phys. Chem. Solids* **1990**, *51*, 239–247. (b) Kohlhaas, T.; Spiering, H.; Gütlich, P. *Z. Phys. B* **1997**, *102*, 455–459. (c) Galet, A.; Gaspar, A. B.; Muñoz, M. C.; Levchenko, G.; Real, J. A. *Inorg. Chem.* **2006**, *45*, 9670–9679. (d) Ksenofontov, V.; Gaspar, A. B.; Levchenko, G.; Fitzsimmons, B.; Gütlich, P. *J. Phys. Chem. B* **2004**, *108*, 7723–7727. (e) Galet, A.; Gaspar, A. B.; Agusti, G.; Muñoz, M. C.; Levchenko, G.; Real, J. A. *Eur. J. Inorg. Chem.* **2006**, 3571–3573.
(22) Slichter, C. P.; Drickamer, H. G. *J. Chem. Phys.* **1972**, *56*, 2142–2161.
(23) Jeftić, J.; Hinek, R.; Capelli, S. C.; Hauser, A. *Inorg. Chem.* **1997**, *36*, 3080–3087.
(24) Adler, P.; Spiering, H.; Gütlich, P. *J. Phys. Chem. Solids* **1989**, *50*, 587–597.

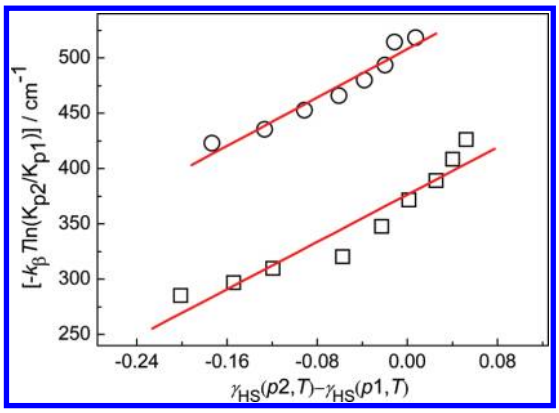

Figure 6. Plots of $[-k_\beta T \ln(K_{p2}/K_{p1})]/cm^{-1}$ versus $\gamma_{HS}(p2,T) - \gamma_{HS}(p1, T)$ for $p1 = 1$ bar and $p2 = 2210$ bar (□) and for $p1 = 1$ bar and $p2 = 4160$ bar (○). Linear fits to the data (—) with $\Delta p = 2210$ and 4160 bar show that slope 2Γ equals 534(6) and 522(5) cm^{-1} and intercept $(\Delta p)\Delta V°_{HL}$ equals 376(6) and 603(5) cm^{-1}, respectively. So, Γ and $\Delta V°_{HL}$ equals 264(5) cm^{-1} and 32(3) $Å^3$ $molecule^{-1}$, respectively.

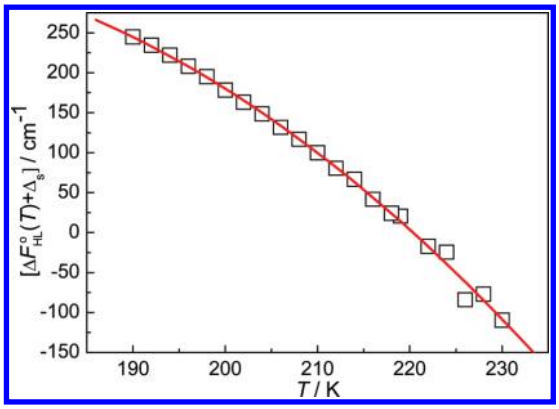

Figure 7. $[\Delta F°_{HL}(T) + \Delta_s]$ versus T plots at 1 bar (□) and the second-order polynomial fit (—).

values of the slope of 534(6) and 522(5) cm^{-1} and intercepts of 376(6) and 603(5) cm^{-1} for $\Delta p = 2210$ and 4160 bar, respectively. So, the corresponding values for Γ and $\Delta V°_{HL}$ are 264(5) cm^{-1} and 32(3) $Å^3$ $molecule^{-1}$, respectively.

Using the calculated values of Γ and $\Delta V°_{HL}$ in eq 5, the sum values of $\Delta F°_{HL}(T) + \Delta_s$ could be obtained from the experimental γ_{HS} data, and the plots of the sum $[\Delta F°_{HL}(T) + \Delta_s]$ versus T at 1 bar are shown in Figure 7. Because of the comparatively strong dependence on the temperature of $\Delta H°_{HL}(T)$ and $\Delta S°_{HL}(T)$ at low temperature,[25] $[\Delta F°_{HL}(T) + \Delta_s]$ does not depend linearly on the temperature. So, instead $[\Delta F°_{HL}(T) + \Delta_s]$ is well described empirically by fitting with a polynomial of second order, which gives the values of $\Delta H°_{HL}(T_{1/2}) + \Delta_s = 12.76$ kJ mol^{-1} and $\Delta S°_{HL}(T_{1/2}) = 59.79$ J mol^{-1} K^{-1}, respectively. The change value of the molar entropy, $\Delta S°_{HL}$ ($T_{1/2}$), is well in line with the general one (50 J mol^{-1} K^{-1}) that is considered to drive the spin transition from the LS to HS state.[26] Using the above values, the calculated spin-transition curves under 1, 2210, and 4160 bar are shown in Figure 8, which are in good agreement with the experimental data.

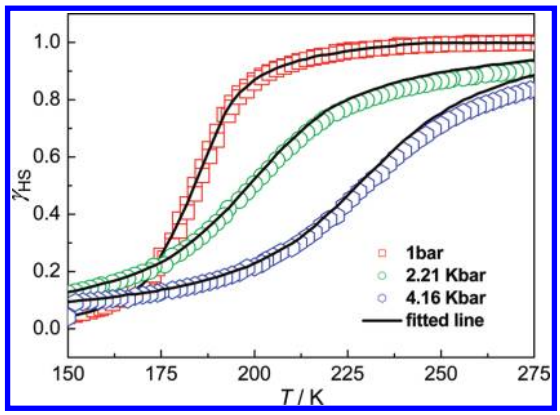

Figure 8. Experimental and calculated HS populations of **1** at 1, 2210, and 4160 bar, respectively.

Meanwhile, a parameter, Π^*, the so-called reduced pressure, which characterizes the type of SCO, has been introduced by Köhler et al.[21]

$$\Pi^* = [\Delta F°_{HL}(T) + \Delta_s + p\Delta V°_{HL}]/\Gamma \quad (7)$$

The spin transition is expected to occur at the critical temperature

$$T_c = \Gamma/2k_\beta \quad (8)$$

If $\Pi^*(T_c) < 1$, a first-order transition with hysteresis is expected, while for $\Pi^*(T_c) > 1$, the transition is continuous and fully reversible. In the present case, the calculated Γ value above (264 cm^{-1}) leads to T_c equal to 191 K according to eq 8, so that Π^* equals 0.42 at 1 bar and, consequently, a first-order transition with a small hysteresis of about 1 K width is observed. At 2.21 and 4.16 kbar, Π^* equals 1.735 and 2.89, respectively; both are larger than 1, giving gradual spin transitions.

Conclusion

Compound **1** exhibits an abrupt and complete spin transition with a small hysteresis, which can be viewed as an ideal candidate to carry out the investigation of pressure effects on the SCO behavior. A directly observed phenomenon is that the transition temperature increases along with an increase of the external pressure. Calculating the magnetic data under different external pressures gives the interaction parameter Γ = 264(5) cm^{-1} and volume change $\Delta V°_{HL}$ = 32(3) $Å^3$ $molecule^{-1}$, respectively, and no direct correlation between Γ and $\Delta V°_{HL}$ is found. The entropy change at 1 bar, $\Delta S°_{HL}(T)$ = 59.79 J mol^{-1} K^{-1}, is a little larger than the theoretical one (50 J mol^{-1} K^{-1}), which is the impetus to drive the spin transition from the LS to HS state.

The results indicate that it is necessary to pay more attention to the pressure effects on SCO because well-developed hydrostatic pressure cells in connection with magnetic susceptibility are available. Some unexpected phenomena in SCO behaviors under external pressure, for instance, the correlation between

(25) (a) Gütlich, P.; Hauser, A.; Spiering, H. *Angew. Chem., Int. Ed. Engl.* **1994**, *33*, 2024–2054. (b) Jung, J.; Bruchhaüser, F.; Feile, R.; Spiering, H.; Gütlich, P. *Z. Phys. B* **1996**, *100*, 517–522. (c) Jung, J.; Schmitt, G.; Wiehl, L.; Hauser, A.; Knorr, K.; Spiering, H.; Gütlich, P. *Z. Phys. B* **1996**, *100*, 523–534. (d) Jakobi, R.; Spiering, H.; Wiehl, L.; Gmelin, E.; Gütlich, P. *Inorg. Chem.* **1988**, *27*, 1823–1827.

(26) (a) Sorai, M. *Top. Curr. Chem.* **2004**, *235*, 153–170. (b) Tuchagues, J. P.; Bousseksou, A.; Molnar, G.; McGarvey, J. J.; Varret, F. *Top. Curr. Chem.* **2004**, *235*, 85–103. (c) Linert, W.; Grunert, M. C.; Koudriavtsev, A. B. *Top. Curr. Chem.* **2004**, *235*, 105–136.

the different shapes of the SCO curves (the presence of unchanged curves against the gradual curves with increasing external pressure) and the special lattice properties such as hydrogen-bonding, $\pi-\pi$ interaction, and crystal-packing effects, are still in the dark.[27] Also, theoretical progress to quantitatively interpret thus unexpected pressure effects would come true if the crystal structure of the SCO compound under different pressures and variable temperature were available.[27]

Experimental Section

Materials and Physical Measurements. All starting materials were obtained commercially and were used without further purification. Elemental analyses for C, H, and N were performed on a Perkin-Elmer 240Q elemental analyzer. The IR spectra (KBr pellets) were recorded in the range of 400−4000 cm^{-1} on a Nicolet 5DX spectrophotometer. Magnetic susceptibility measurements were carried out at a sweeping rate of 1 K min^{-1} in the temperature range of 2−300 K with a magnetic field of 5000 Oe on a Quantum Design MPMS XL-7 magnetometer. The magnetic measurements under pressure were performed by using an EasyLab Mcell 10 hydrostatic pressure cell,[28] which is specially designed for the MPMS setup and made of hardened beryllium bronze with silicon oil as a pressure-transmitting medium. The applied pressure was measured by using the pressure dependence of the superconducting transition temperature of a built-in pressure sensor made of high-purity tin. Magnetic data were calibrated with the sample holder and diamagnetic contributions. The ligand pmea was synthesized by a literature method.[29]

Preparation of [Fe(pmea)(NCS)$_2$] (1). First, a powder sample was synthesized as follows: $FeSO_4 \cdot 7H_2O$ (0.1 mmol) and KSCN (0.2 mmol) were dissolved in 5 mL of methanol, and 5 mg of ascorbic acid was added into the solution to avoid oxidation of the Fe^{II} ion. Then, the solution was filtered to remove the precipitate of K_2SO_4, an ethanol solution (10 mL) containing pmea (0.1 mmol), and 5 mg of ascorbic acid was added into the filtrate immediately under stirring and nitrogen. The powder products precipitated and were filtered. Second, 30 mg of powder **1** was dissolved in a 1 mL DMF solution, and the solution was layered with ethanol to give light-yellow blocklike single crystals of **1** in 60% yield. Anal. Calcd for $C_{21}H_{20}N_6S_2Fe$: C, 52.95; N, 17.64; H, 4.23. Found: C, 53.17; N, 17.82; H, 3.89. IR (KBr, cm^{-1}): 2075, 2064, 1602, 1571, 1484, 1439, 1308, 1153, 1103, 1018, 758.

Crystallographic Studies. Diffraction data of **1** (0.50 × 0.20 × 0.15 mm) were collected on an Oxford Gemini S Ultra diffractometer with a Mo Kα (λ = 0.710 73 Å) source. Single crystals were first cooled to 120 K in a flow of liquid nitrogen, and data were collected at this temperature. After that, the sample was warmed to 260 K, followed by the collection of a second data set. Empirical absorption corrections were applied to all data using CrysAlis RED.[30] The structures were solved by direct methods and refined by full-matrix least-squares calculations (F^2) with *SHELXS-97* and *SHELXL-97*,[31] respectively. All non-H atoms were anisotropically refined, and H atoms were generated using the riding model.

Compound **1**: $C_{21}H_{20}N_6S_2Fe$, M = 476.4, orthorhombic, $Pc2_1n$. T = 120(2) K, a = 10.451(1) Å, b = 13.313(1) Å, c = 14.991(1) Å, V = 2085.7(1) $Å^3$, Z = 4, D_c = 1.517 Mg m^{-3}, R1 = 0.0234, wR2 (all data) = 0.0575, μ = 0.945 mm^{-1}, S = 1.004. T = 260(2) K, a = 10.828(2) Å, b = 13.653(2) Å, c = 15.313(3) Å, V = 2263.8(6) $Å^3$, Z = 4, D_c = 1.398 Mg m^{-3}, R1 = 0.0344, wR2 (all data) = 0.0739, μ = 0.870 mm^{-1}, S = 0.917.

Acknowledgment. This work was supported by the NNSF of China (Grants 90922012, 20971106, and 20721001), NCET-08-0470 of MOE, the NSF of Fujian Province (Distinguished Young Scientists Grant 2009J06006), and the 973 project (Grant 2007CB815301).

Supporting Information Available: Crystallographic information in CIF format. This material is available free of charge via the Internet at http://pubs.acs.org.

(27) Gütlich, P.; Ksenofontov, V.; Gaspar, A. B. *Coord. Chem. Rev.* **2005**, *249*, 1811–1829.
(28) easyLab Technologies Limited. easyLab Mcell 10−10 kbar hydrostatic pressure cell for a Quantum Design MPMS measurement platform.
(29) Schatz, M.; Becker, M.; Thaler, F.; Hampel, F.; Schindler, S.; Jacobson, R. R.; Tyeklar, Z.; Murthy, N. N.; Ghosh, P.; Chen, Q.; Zubieta, J.; Karlin, K. D. *Inorg. Chem.* **2001**, *40*, 2312–2322.
(30) *CrysAlisPro*, version 1.171.33.34d; Oxford Diffraction Ltd.: Oxfordshire, U.K., **2009**.
(31) (a) Altomare, A.; Burla, M. C.; Camalli, M.; Cascarano, G. L.; Giacovazzo, C.; Guagliardi, A.; Moliterni, A. G. G.; Polidori, G.; Spagna, R. *J. Appl. Crystallogr.* **1999**, *32*, b115–119. (b) Sheldrick. G. M. *SHELXL-97, Program for refinement of crystal structures*; University of Göttingen: Göttingen, Germany, **1997**.